

# On the Invariant Distribution of Galaxies in the $r_e - \langle \mu \rangle_e$ plane out to $z = 0.64$

F. La Barbera, G. Busarello, P. Merluzzi, M. Massarotti

and

M. Capaccioli

labarber@na.astro.it

*INAF Osservatorio Astronomico di Capodimonte, Napoli, Italy*

## ABSTRACT

This work deals with the evolution of the relation between half-light (effective) radius,  $r_e$ , and mean surface brightness,  $\langle \mu \rangle_e$ , (known as Kormendy relation) at intermediate redshifts. A large sample of spheroids ( $N \sim 230$ ) in the three clusters of galaxies A 209 at  $z = 0.21$ , AC 118 at  $z = 0.31$ , and EIS 0048 at  $z = 0.64$  is analyzed by using ground-based data. Effective parameters have been derived in the R-band for A 209 and AC 118, and in the I-band for EIS 0048, covering closely the same V-band restframe. The slope,  $\beta$ , the intrinsic dispersion,  $\sigma_{\langle \mu \rangle_e}^{(i)}$ , and the zeropoint,  $\alpha$ , of the  $r_e - \langle \mu \rangle_e$  relation are obtained by a fitting procedure accounting for the selection criteria of the samples. The slope of the Kormendy relation for the three clusters turns out to be the same at all redshifts: we obtain  $\beta = 2.91 \pm 0.08$ . We show that this result constrains the formation epoch of galaxy stellar populations to change by less than 18–28% per decade of galaxy radius. Moreover, the intrinsic dispersion of the relation does not vary with redshift,  $\sigma_{\langle \mu \rangle_e}^{(i)} = 0.31 \pm 0.04$ , and the distributions of galaxies in the plane of the effective parameters do not vary from cluster to cluster, as proven by the Kolmogorov–Smirnov test. We conclude that, whatever the mechanism driving galaxy evolution is, it does not affect significantly the properties of bright galaxies in the  $\log r_e - \langle \mu \rangle_e$  plane at least from  $z = 0.64$  to date. The evolution of the zeropoint is compared with predictions of stellar population models: consistently with previous studies, the observed trend can be explained by a pure Tolman signal superposed to the luminosity evolution of stellar populations having a high formation redshift ( $z_f > 2$ ).

*Subject headings:* Galaxies: evolution – Galaxies: fundamental parameters (effective radii, mean surface brightness) – Galaxies: clusters: individual: A 209, AC 118, EIS 0048 – Galaxies: statistics – Galaxies: photometry

## 1. Introduction

Early-type galaxies (ETGs) are known to populate a two-dimensional manifold in the space of their observed quantities. This Fundamental Plane (FP) is usually expressed by a correlation among the effective radius  $r_e$ , the mean surface brightness  $\langle \mu \rangle_e$  within  $r_e$ , and the central velocity dispersion  $\sigma_0$ :

$$\log r_e = a \cdot \log \sigma_0 + b \cdot \langle \mu \rangle_e + c. \quad (1)$$

Due to the small intrinsic dispersion ( $\sim 10\%$  in  $r_e$  and  $\sigma_0$ , and  $\sim 0.1$  mag in  $\langle \mu \rangle_e$ ), the FP is considered as a powerful tool to measure galaxy distances and to constrain the processes driving galaxy evolution (e.g. Kjærgaard, Jørgensen, and Moles 1993; Jørgensen, Franx, and Kjærgaard 1996; Jørgensen et al. 1999; Kelson et al. 2000).

A tight projection of the FP is the correlation between  $R_e$  and  $\langle \mu \rangle_e$ , also known as Kormendy relation (hereafter KR):

$$\langle \mu \rangle_e = \alpha + \beta \cdot \log R_e, \quad (2)$$

where  $R_e$  is the effective radius in kpc, and  $\beta \simeq 3$  (Kormendy 1977). Different studies have demonstrated that in the nearby universe bright ETGs define a sharp sequence in the  $\log R_e - \langle \mu \rangle_e$  plane, with an intrinsic dispersion of  $\sim 0.3 - 0.4$  in  $\langle \mu \rangle_e$  (Hamabe and Kormendy 1987; Hoessel, Oegerle, and Schneider 1987; Sandage and Perelmuter 1991; Sandage and Lubin 2001). Moreover, Capaccioli, Caon, and D’Onofrio (1992) have shown that ETGs + bulges form two distinct families in the plane of the effective parameters: that of the bright ETGs, following the KR, and another ‘ordinary’ family, whose properties are more disperse and heterogeneous.

In order to understand the processes underlying galaxy formation and evolution, it is relevant to investigate the FP scaling relations at different lookback times. In the monolithic formation scenario (Larson 1974), ETGs form at very high redshifts in a strong burst of star formation, and the distribution of galaxies in the space of observed quantities changes with redshift due to the passive fading of their stars. In the hierarchical framework, bright ETGs form by the progressive merging of smaller units, and the FP relations are built up with redshift. Different works have shown (1) that (dissipation-less) merging seems to move galaxies along the FP (Capelato, de Carvalho, and Carlberg 1995; Dantas et al. 2002), and (2) that in hierarchical models, the luminosity-weighted ages of stellar populations in cluster galaxies appear to be the same of those predicted for pure passive evolution (e.g. Kauffmann 1996). All these facts suggest that for both scenarios dynamical effects could play a minor role in the evolution of FP correlations. It is expected that the FP slopes change with redshift mainly for possible differences in properties of galaxy stellar populations (such as age and

metallicity) along the early-type sequence, while the zero point varies consistently with the evolution of a passive stellar population. In the hierarchical framework, however, it is also expected that the distribution in the space of observed quantities evolves with redshift, as merging proceeds to larger and larger sizes. Clearly, in order to analyze this subject, large samples of galaxies are needed at different lookback times.

In the recent years, it has become feasible to study the FP scaling relations of galaxies at intermediate redshifts. Due to the heavy request of observing time needed for velocity dispersion measurements, many studies have investigated pure photometric projections of the FP, like the KR. The main effort to constrain the evolution of the KR slope with redshift has been performed by Ziegler et al. (1999), who analyzed ETGs properties in four clusters at  $z \sim 0.4$  and in one at  $z = 0.55$ , with an average of  $\sim 20$ – $30$  galaxies per cluster. These authors found that the slope is comprised between 2.2 and 3.5 both for the Coma and for the distant clusters, depending on the selection criteria of the samples, and suggested, therefore, that it could not have evolved since  $z \sim 0.55$ .

The evolution of the KR zero point for cluster galaxies has been investigated by different works in order to perform the Tolman surface brightness test for the universal expansion (Sandage and Perelmuter 1991; Pahre, Djorgovski, and de Carvalho 1996; Sandage and Lubin 2001; Lubin and Sandage 2001a,b,c) and to derive the luminosity evolution of ETGs (e.g. Barger et al. 1998; Ziegler et al. 1999). They concluded that the measured change is consistent with what expected on the basis of cosmological dimming plus passive aging of stellar populations formed at high redshifts.

The KR was investigated up to  $z \sim 2 - 3$  for field galaxies in the Hubble Deep Field by Fasano et al. (1998).

As shown by La Barbera et al. (2002a), it is possible to derive structural parameters of galaxies at intermediate redshifts by using ground-based imaging. In the present work, we use structural parameters in the V-band restframe for a total of  $N \sim 230$  spheroids in the clusters A 209 at  $z = 0.21$ , AC 118 at  $z = 0.31$ , and EIS 0048 at  $z = 0.64$ , and investigate the evolution of the distributions in the  $\log r_e - \langle \mu \rangle_e$  plane up to a lookback time of  $\sim 6$  Gyr. A suitable fitting procedure is introduced, that accounts for the selection criteria of each sample, providing an un-biased estimate of the KR coefficients with redshift.

The layout of the paper is the following. Section 2 describes the samples used for the present analysis. Section 3 deals with the evolution of the KR slope and the comparison of the  $\log r_e - \langle \mu \rangle_e$  distributions at different redshifts, and section 4 shows the luminosity evolution inferred by the KR. Conclusions are drawn in section 5. In the following, we will assume the cosmology  $\Omega_m = 0.3$ ,  $\Omega_\Lambda = 0.7$  and  $H_0 = 70 \text{ Kms}^{-1}\text{Mpc}^{-1}$ . With this parameters, the age

of the universe is  $\sim 13.5$  Gyr, and the redshifts  $z = 0.21$ ,  $z = 0.31$ , and  $z = 0.64$  correspond to lookback times of  $\sim 2.5$ ,  $3.5$ , and  $6$  Gyr respectively.

## 2. The samples

Photometry for the three clusters of galaxies A 209 ( $z = 0.21$ ), AC 118 ( $z = 0.31$ ), and EIS 0048 ( $z = 0.64$ ) resides on data collected at the ESO New Technology Telescope (NTT) and at the ESO Very Large Telescope (VLT). The data relevant for the present study include images in the R-band for A 209 and AC 118, and in the I-band for EIS 0048, all corresponding approximately to V-band restframe. For AC 118 and EIS 0048, galaxies were selected according to the photometric redshift technique (see Massarotti et al. 2001, and references therein), while for A 209, we considered the sample of spectroscopically confirmed cluster members from Mercurio et al. (2002) complemented with photometric data (see below). The relevant information on the samples are summarized in table 1.

Structural parameters were derived as described in La Barbera et al. (2002a), by fitting galaxy images with Sersic models convolved with suitable representations of the PSF. Uncertainties on structural parameters were estimated as described in La Barbera et al. (2002c), and amount to  $\delta(\log r_e) \sim 0.09$  and  $\delta(\langle \mu \rangle_e) \sim 0.4$  for A 209,  $\delta(\log r_e) \sim 0.14$  and  $\delta(\langle \mu \rangle_e) \sim 0.55$  for AC 118, and to  $\delta(\log r_e) \sim 0.07$  and  $\delta(\langle \mu \rangle_e) \sim 0.30$  for EIS 0048. In order to study the KR relation, we selected the population of spheroids on the basis of the shape of the light profile, as parametrized by the Sersic index  $n$ . We classified as spheroids the galaxies with  $n > 2$ , corresponding to objects with a bulge fraction greater than  $\sim 20\%$  (see van Dokkum et al. 1998; Saglia et al. 1997). For each cluster we considered all the galaxies brighter than a given magnitude limit  $m_c$ . In order to exclude few objects with small radii and poorly determined structural parameters, we selected only galaxies with  $\langle \mu \rangle_e$  greater than a given surface brightness limit  $\langle \mu \rangle_{e,c}$ . The completeness of the spectroscopic sample of A 209 is about 50% at  $R \sim 20$ , and falls to zero at  $R = 21$ . In order to obtain a magnitude limited sample we added to the spectroscopic data all the spheroids within the colour–magnitude sequence of A 209 (see Mercurio et al. 2002) down to  $R \sim 20.5$ . We point out that the present samples constitute the largest data set ( $N \sim 230$ ) of cluster galaxies, for which the Kormendy relation is investigated up to a lookback time of  $\sim 6$  Gyr.

In order to compare the distributions in the  $\log r_e - \langle \mu \rangle_e$  plane at intermediate redshifts with that of nearby galaxies, we took advantage of the large sample ( $N = 147$ ) of ETGs in the Coma cluster by Jørgensen, Franx, and Kjørgaard (1995a,b, hereafter JFK95a and JFK95b). Structural parameters were taken by JFK95a, who fitted the growth curve of aperture magnitudes with de Vaucouleurs  $r^{1/4}$  profiles and corrected the estimated parame-

ters for seeing effects. The typical uncertainties of  $\log r_e$  and  $\langle \mu \rangle_e$  amount to  $\sim 0.08$  and  $\sim 0.3$  mag, respectively (see table 11 of JFK95a). Since it was not possible to select galaxies in the JFK95a sample by using Sersic indices as for the other clusters, we adopted the relation between Sersic index and central velocity dispersion recently found for nearby galaxies by Graham (2002):  $\log n \propto \log \sigma_0$ . We considered only the sample of Coma ETGs with available velocity dispersion measurements from JFK95b, selecting galaxies with  $\sigma_0 > 110 \text{ km s}^{-1}$ , that corresponds to  $n \gtrsim 2$  (see Figure 1 of Graham 2002). We also excluded from the calculation of the fitting coefficients the five galaxies with largest size in the JFK95a sample: due to the presence of extended halos the use of a de Vaucouleurs model can give very different parameters with respect to those estimated by the Sersic models. The final sample consists in  $N = 72$  galaxies and is complete down to  $r_G \sim 15.3$ , where  $r_G$  is the Thuan–Gunn r-band magnitude. Since spheroids have very small internal colour gradients at optical wavelengths, the difference between the  $r_G$  band and the V-band restframe at the Coma redshift is not relevant for the present study.

For A 209, AC 118, and EIS 0048 mean surface brightnesses were corrected for galactic extinction following Schlegel, Finkbeiner, and Davis (1998), while cosmological dimming was not removed. For the Coma sample, since both corrections were applied by JFK95a, we added the term  $10 \cdot \log(1 + z)$  to the  $\langle \mu \rangle_e$  values.

### 3. Kormendy relations

The  $\log r_e - \langle \mu \rangle_e$  diagrams for Coma, A 209, AC 118, and EIS 0048 are shown in Figure 1. For each cluster, spheroids follow a sharp, well defined KR in the region defined by the selection limits.

#### 3.1. Fitting the KR

The  $\log r_e - \langle \mu \rangle_e$  sequences were fitted by applying a modified least square procedure (hereafter MLS), taking into account the completeness cuts in magnitude and  $\langle \mu \rangle_e$ . The fitting coefficients were derived by minimizing the rms of the residuals with respect to  $\log r_e$  and  $\langle \mu \rangle_e$  (MLS <sub>$\log r_e$</sub>  and MLS <sub>$\langle \mu \rangle_e$</sub>  fits), and by applying the bisector regression (BMLS, see Akritas and Bershady 1996). Details can be found in appendix A.

An important point in the fit of FP scaling relations is the correlation between the uncertainties on galaxy parameters: for the effective parameters, we have  $\delta(\log r_e) = \gamma \cdot \delta(\mu_e)$  (see JFK95a), where the value of  $\gamma$  depends on the methods used to derive  $r_e$  and  $\langle \mu \rangle_e$ , and

the corresponding uncertainties. In order to estimate the range of possible values for  $\gamma$ , we compared the uncertainties on  $\log r_e$  and  $\langle \mu \rangle_e$  for sample of galaxies from different sources (Lucey, Bower, and Ellis 1991; Saglia, Bender, and Dressler 1993; Jørgensen, Franx, and Kjaergaard 1995a; Scodreggio, Giovanelli, and Haynes 1997; Scodreggio, Gavazzi, and Belsole 1998; Mobasher et al. 1999): we found  $0.25 \lesssim \gamma \lesssim 0.34$ . By using numerical simulations (see La Barbera et al. 2002a) and by comparing repeated measurements of  $r_e$  and  $\langle \mu \rangle_e$  (see La Barbera et al. 2002c), we obtained  $\gamma \sim 0.25$  for the parameters of A 209, AC 118, and EIS 0048, in agreement with the quoted range of  $\gamma$  values. The correlation between  $\delta(\log r_e)$  and  $\delta(\langle \mu \rangle_e)$  and the typical values of the uncertainties on the effective parameters (see section 2) are shown in Figure 1. The effect on the KR coefficients was estimated by using numerical simulations of the  $\log r_e - \langle \mu \rangle_e$  diagrams, performed by an analogous procedure to that described in La Barbera, Busarello, and Capaccioli (2000) for the Fundamental Plane. We found that the bias on the KR coefficients is negligible, amounting at most to  $\sim 3\%$  for the KR slope of AC 118. This is in agreement with what found by Hamabe and Kormendy (1987) for the  $\log r_e - \langle \mu \rangle_e$  relation of nearby bright ellipticals and spiral bulges.

### 3.2. Evolution of the slope

The slopes,  $\beta$ , of the KRs are reported in table 2, while the variation of  $\beta$  with redshift is shown in Figure 2. The uncertainties were estimated by the bootstrap method and amount to  $\sim 4-6\%$  for A 209, AC 118, and EIS 0048. We notice that the uncertainty for the Coma sample is significantly higher ( $\sim 10 - 15\%$ ) due to the smaller range of  $\log r_e$  considered in the fit. Figure 2 clearly shows that the values of  $\beta$  are fully consistent for each pair of clusters, except for the  $\text{MLS}_{\log r_e}$  and  $\text{MLS}_{\langle \mu \rangle_e}$  slopes of the Coma cluster, that are consistent with the other values at a lower significance level ( $\sim 1.5 \div 2 \sigma$ ). However, this is due to the fact that the  $\text{MLS}_{\log r_e}$  and  $\text{MLS}_{\langle \mu \rangle_e}$  methods are more sensitive, with respect to the BMLS method, to the range of  $\log r_e$  used in the fit<sup>1</sup>. We conclude, therefore, that no significant evolution in the slope of the KR is found up to  $z \sim 0.64$ . The weighted means of  $\beta$ , reported in table 3 for each fitting procedure, are in very good agreement with the value of 2.94 derived by Hamabe and Kormendy (1987) and with the values of the KR slopes obtained recently by Sandage and Lubin (2001) for nearby galaxies ( $2.9 \lesssim \beta \lesssim 3.4$ ).

The evolution of the KR slope with redshift,  $\Delta(\beta)$ , carries information on the variation of the properties of stellar populations (SPs) along the galaxy sequence, as shown by the

---

<sup>1</sup>In fact, if we include also the five largest galaxies in the fit of the Coma sample, the bisector method gives  $\beta = 2.3 \pm 0.4$ , that is fully consistent with the value in table 2.

following relation:

$$\Delta(\beta) = \Delta \left( \frac{d\langle\mu\rangle_e}{d\log r_e} \right) = \frac{d\Delta(\langle\mu\rangle_e)}{d\log r_e} = \frac{dE}{d\log r_e}, \quad (3)$$

where  $E = E(r_e)$  is the luminosity evolution between  $z = 0.64$  and  $z = 0$  at a given radius  $r_e$ . In appendix B, we use the GISSEL98 synthesis code (Bruzual and Charlot 1993) to derive an approximated analytic expression for  $E$  as a function of the age  $t_f$  and the metallicity  $Z$  of the galaxy SPs. We consider luminosity evolution in the V-band, since (1) the filters relative to each sample approximate the V-band restframe and (2) internal colour gradients of spheroids are known to be very small in the optical and not to evolve significantly at intermediate redshifts (see La Barbera et al. 2002c). For models with formation redshift  $z_f \in [1.8, 10]$  and  $Z \in [0.2, 2.5]Z_\odot$ , that are suitable to describe the population of spheroids (see also section 4), we show that  $E$  depends mainly on  $t_f$ , i.e.  $E \simeq E(t_f)$ , and that, therefore, Eq. 3 can be approximated as:

$$\Delta(\beta) \simeq \frac{dE}{d\log t_f} \cdot \frac{d\log t_f}{d\log r_e} = F(t_f) \cdot \frac{d\log t_f}{d\log r_e}. \quad (4)$$

where  $F(t_f) = dE/d\log t_f$  is computed as described in appendix B. Assuming that the maximum allowed variation of  $\beta$  is  $2\sigma_\beta$  (see table 3), we obtain the relation

$$|d\log t_f/d\log r_e| < 2\sigma_\beta/F(t_f). \quad (5)$$

For a SSP we find  $F(t_f) \in [1.3, 1.65]$  mag/Gyr, and the value of  $2\sigma_\beta/F(t_f)$  turns out to be in the range  $[0.1, 0.12]$ . This implies that the absolute relative variation of  $t_f$  per decade of galaxy radius must be smaller than  $\sim 28\%$  ( $\sim 0.12$  dex). As shown in appendix B, a lower limit is obtained for SP models with a protracted SFR. For an exponential SFR with time scale  $\tau = 1$  Gyr, we find  $F(t_f) \in [2, 3]$  mag/Gyr and the relative variation of  $t_f$  is constrained to be smaller than  $\sim 18\%$ .

### 3.3. Evolution of the intrinsic dispersion

Since the values of  $\beta$  are the same at all redshifts, we adopted as common slope in the KR fit the value relative to the BMLS regression, and computed for each sample the zeropoint  $\alpha$  and the scatter  $\sigma_{\langle\mu\rangle_e}$ , defined by the rms of residuals in  $\langle\mu\rangle_e$ . The uncertainties on  $\alpha$  and  $\sigma_{\langle\mu\rangle_e}$  were obtained by numerical simulations, by taking also into account the measurement error on the adopted value of the slope. We estimated the intrinsic dispersion of the relations ( $\sigma_{\langle\mu\rangle_e}^{(i)}$ ) by subtracting in quadrature to  $\sigma_{\langle\mu\rangle_e}$  the typical uncertainty on  $\langle\mu\rangle_e$  (see section 2). The values are given in table 4. It is clear from the table that the

KR has significant intrinsic dispersion also at intermediate redshifts ( $\sim 0.3$  in  $\langle \mu \rangle_e$ ), and that this dispersion does not change with redshift. The intrinsic dispersion of the KR is consistent with that reported by Hoessel, Oegerle, and Schneider (1987) and Kjærgaard, Jørgensen, and Moles (1993) for nearby galaxies, and is mainly due to neglecting velocity dispersions in the FP relation (Eq. 1).

### 3.4. Comparison of the distributions of effective parameters

To compare the distributions in the  $\log r_e - \langle \mu \rangle_e$  plane, we shifted the values of  $\langle \mu \rangle_e$  for A 209, AC 118, and EIS 0048 by matching the zeropoints of the KR. The Coma cluster was not considered in order to compare only the clusters with structural parameters derived by the same procedure. The combined  $\log r_e - \langle \mu \rangle_e$  diagram for A 209, AC 118, and EIS 0048 is shown in Figure 3. We checked the hypothesis that each pair of samples comes from the same parent distribution by performing the two-dimensional Kolmogorov–Smirnov (KS) test (Fasano and Franceschini 1987). The test was repeated by using different shifts for each cluster to take into account the uncertainties on  $\alpha$  reported in table 4, by applying the same magnitude cut to each sample. We found significance levels of the KS statistics between 10% and 25% by comparing AC 118 with the other two clusters, and a larger significance level ( $\sim 50\%$ ) by comparing A 209 and EIS 0048. We point out that the result for A 209 and EIS 0048 is of particular interest, since the measurement uncertainties for these clusters are similar and are comparable with the intrinsic dispersion of the KR. Since the error bars for the AC 118 data are significantly larger, we also performed the KS test by adding further scatter to the  $\log r_e - \langle \mu \rangle_e$  diagram of A 209 and EIS 0048 in order to mimic the measurement uncertainties on the effective parameters of AC 118. In this case, we obtained higher significance levels of the KS test: between 50% and 80%.

The previous results suggest that the distributions in the  $\log r_e - \langle \mu \rangle_e$  plane are not significantly changed at least since  $z \sim 0.64$ .

## 4. Luminosity evolution

The evolution of the zeropoint of the KR with redshift is determined (1) by the effect of the cosmological dimming on  $\langle \mu \rangle_e$ , (2) by the luminosity evolution of galaxy stellar populations, (3) by the values of cosmological parameters. Since the investigation of point (3) would require a larger number of cluster samples, we will focus the discussion on points (1) and (2).

We applied suitable corrections to the data in order to convert the  $\langle \mu \rangle_e$  values to the same restframe, V-band, for each cluster. We used the GISSEL98 synthesis code (Bruzual and Charlot 1993) to construct galaxy templates with different age  $t_0$ , metallicity  $Z$  and time scale  $\tau$  of star formation. In order to consider a wide range of possible spectral types describing galaxies in our samples, we chose the following range of parameters:  $t_0 \in [8, 13]$  Gyr,  $Z \in [0.5, 1.5]Z_\odot$  and  $\tau \in [0.01, 5]$  Gyr. The mean values of the derived corrections and the relative uncertainties are shown in table 5. We notice that the uncertainties are very small ( $\lesssim 0.03$  mag), i.e. the dependence on the spectral type is negligible, due to the fact that the observed wavebands approximate closely the V-band restframe for each cluster. We also verified that using SSP spectra by Buzzoni (1989) gives values fully consistent with those of table 5. This proves that it is suitable to apply the same corrections to all the galaxies in each cluster. The V-band zeropoints ( $\langle \mu_V \rangle_e$ ) of the KR were obtained by adding the values reported in table 5 to the values of  $\alpha$  (table 4), and the corresponding error budgets were estimated by adding in quadrature the uncertainties on the corrections with  $\sigma_\alpha$ .

In Figure 4 we show the relation between  $\langle \mu_V \rangle_e$  and  $\log(1+z)$ . The observed points are well described by a linear relation  $\langle \mu_V \rangle_e = \Gamma \cdot \log(1+z)$ . A least square fit gives  $\Gamma = 7.22 \pm 0.6$ , or equivalently:  $\langle I_V \rangle_e \propto (1+z)^{-2.88 \pm 0.24}$ , where  $\langle I_V \rangle_e$  is the mean surface brightness within  $r_e$  in linear units. As definitively shown by Lubin and Sandage (2001c), this excludes the relation  $\langle I_V \rangle_e \propto (1+z)^{-1}$ , that would hold in the case of a non-expanding universe. We compare the relation between  $\langle \mu_V \rangle_e$  and  $\log(1+z)$  with a no evolution sequence, that is with a pure Tolman signal  $\langle I_V \rangle_e \propto (1+z)^{-4}$ , and with pure luminosity evolution models (see Figure 4). These models were constructed by the GISSEL98 synthesis code: we considered galaxy templates with solar metallicity  $Z = Z_\odot$ , with different formation redshifts ( $z_f = 1, 2, 5, 10$ ), and with two time scales of star formation:  $\tau = 1$  Gyr, that gives a suitable description of the evolution of ETG’s integrated colours, and  $\tau = 0.01$  Gyr, that reproduces the properties of a simple stellar population. Changing the value of  $Z$  in the range  $0.5\text{--}1.5Z_\odot$  does not vary significantly the results. The models were arbitrarily scaled, in order that the ‘pure dimming’ sequence matches the value for the Coma redshift.

According to what found by previous studies (see Lubin and Sandage 2001c), the trend of  $\langle \mu \rangle_e$  with redshift is well described by the superposition of the Tolman signal with pure (passive) luminosity evolution. The formation redshift of the stellar populations is constrained to be higher than  $z_f \sim 2$  with a confidence level  $\gtrsim 2\sigma$  (see Barger et al. 1998; Ziegler et al. 1999).

## 5. Conclusions

We have studied the evolution of the optical, restframe V-band, Kormendy relation in the range  $0 \lesssim z \lesssim 0.64$ , by using ground-based effective parameters derived in previous works for the clusters of galaxies A 209 ( $z = 0.21$ ), AC 118 ( $z = 0.31$ ), and EIS 0048 ( $z = 0.64$ ), and published data for the Coma cluster ( $z \sim 0.023$ ). Galaxies were selected by the photometric redshift technique for AC 118 and EIS 0048 and by spectroscopic redshifts complemented with photometric data for A 209.

The results of the present work can be summarized as follows.

- Spheroids define a tight, well defined, sequence in the plane of the effective parameters at least back to  $z \sim 0.64$ .
- We introduce a fitting procedure for the KR that takes into account the selection effects (such as the magnitude cut) in the  $\log r_e - \langle \mu \rangle_e$  plane. The slope  $\beta$  and the intrinsic dispersion  $\sigma_{\langle \mu \rangle_e}^{(i)}$  turn out to be consistent at all redshifts. The mean values of  $\beta$  and  $\sigma_{\langle \mu \rangle_e}^{(i)}$  are  $2.91 \pm 0.08$  and  $0.31 \pm 0.04$ , respectively.
- The fact that the KR slopes are the same among all the clusters constrains the possible change in the formation epoch of galaxy stellar populations per decade of radius. We show that the relative variation has to be smaller than  $\sim 28\%$  for SSP models, and smaller than  $\sim 18\%$  for populations having an exponential SFR with  $\tau = 1$  Gyr.
- The two-dimensional Kolmogorov–Smirnov test shows that the distribution in the  $\log r_e - \langle \mu \rangle_e$  plane is consistent for each pair of cluster.
- As found by previous studies, the evolution of the KR zeropoint is explained with the superposition of the Tolman signal and the passive evolution of stellar populations with high formation redshift,  $z_f > 2$ .

The previous points imply that, whatever the mechanism driving galaxy evolution is, (1) it has already built up the Kormendy relation at  $z = 0.64$  and (2) it does not affect significantly the properties of spheroids in the plane of effective parameters from that redshift down to  $z \sim 0$ . The fact that the KR slope does not evolve with redshift sets constraints on the differential luminosity evolution along the early-type sequence, and, therefore, on the properties of galaxy stellar populations as a function of galaxy radius (see also Ziegler et al. 1999). These results should be taken into account by any model aimed at reproducing the physical processes underlying formation and evolution of spheroids.

The present work proves that ground-based data are an effective tool to investigate pure photometric scaling laws, such as the Kormendy relation, at intermediate redshifts. This allows us to study very large samples of galaxies and to take advantage of different wavelength ranges. In a forthcoming paper, we will present the KR study for a large sample of cluster galaxies, with surface photometry derived in the K-band. This is of particular interest, since the NIR is less sensitive to recent episodes of star formation and, therefore, follows more closely the mass distribution in galaxies.

We are grateful to R. de Carvalho and A. Iovino for the helpful discussions. We thank A. Mercurio for providing us with the photometry of the cluster of galaxies A 209. Michele Massarotti is partly supported by a ‘MIUR-COFIN’ grant.

### A. The MLS fits

We consider the statistical model:

$$Y = A + B \cdot X \tag{A1}$$

where  $X$  and  $Y$  are two random variables describing the distributions of  $\log r_e$  and  $\langle \mu \rangle_e$  (or viceversa) and  $A$  and  $B$  are the zero point and the slope of the KR. In order to derive  $A$  and  $B$ , we have to take into account the constrains on  $X$  and  $Y$  deriving from the selection cuts. By considering the case of a single cut, we have the following constrain:

$$y < c_1 + c_2 \cdot x \tag{A2}$$

where  $x$  and  $y$  are the outputs of  $X$  and  $Y$ , while the coefficients  $c_1$  and  $c_2$  describe the selection cut. The direction of the inequality in Eq. A2 is chosen arbitrarily. In the case of the magnitude limit  $m_c$ , with  $x = \log r_e$  and  $y = \langle \mu \rangle_e$ , we have  $c_1 = m_c + 2.5 \cdot \log(2\pi)$  and  $c_2 = 5$ . This follows from the relation  $m_T = -2.5 \cdot \log(2\pi) - 5 \cdot \log r_e + \langle \mu \rangle_e$ , where  $m_T$  is the total magnitude, and from the constrain  $m_T < m_c$ .

For a fixed value of  $x$ , the probability of finding a point in the interval  $(y, y + dy)$  is given by

$$P_x(y)dy = K(A, B, c_1, c_2) \cdot \exp \left[ -(y - A - B \cdot x)^2 / (2\sigma^2) \right] \cdot f(c_1 + c_2 \cdot x - y) \tag{A3}$$

where  $f$  is a step function, and the coefficient  $K$  is derived by imposing  $\int P(y)dy = 1$ . Eq. A3 can be directly generalized to the case of multiple cuts and to a more complex shape of the selection function  $f$ . We write the likelihood  $L = \prod P_{x_i}(y_i)$ , and derive the coefficients in

Eq. A1 by minimizing the function  $-\ln L$  with respect to A and B. We notice that in the ordinary least square fit the function  $f$  is absent in Eq. A3. Therefore, the term K does not depend on A and B and the minimization of  $-\ln L$  reduces to solving a coupled system of linear equations in A and B.

## B. Parameterizing the luminosity evolution

Spectra of galaxy templates were constructed by the GISEL98 synthesis code, considering models with a Scalo IMF and an exponential SFR,  $e^{-t/\tau}$ . We considered SSP spectra and models having a protracted SFR,  $\tau = 1.0$  Gyr, with metallicity  $Z = 0.2, 0.4, 1, 2.5 Z_{\odot}$  and age  $t_f \in [4, 13]$  Gyr. The range of  $t_f$  was chosen in order to describe the properties of galaxy templates having formation redshift  $z_f \in [1.8, 10]$  (corresponding to a lookback time  $t_{LB} \in [10, 13]$  Gyr), from  $z = 0.64$  to  $z = 0$ .

For both models, we found that the dependence of the V-band magnitude at  $z \sim 0$  on  $t_f$  and  $Z$  is well described by a second-order polynomial fit:

$$m_V(t_f, Z) \simeq \sum_{i=1,2} c_i \cdot [\log t_f]^i + \sum_{i=1,2} d_i \cdot [\log Z]^i + \text{const}, \quad (\text{B1})$$

with a rms of  $\sim 0.02$  mag. The magnitude  $m_V$  at  $z = 0.64$  is obtained by substituting  $t_f$  with  $t_f - t_{0.64}$  in Eq. B1, where  $t_{0.64}$  is the lookback time corresponding to  $z = 0.64$ . We point out that the presence of cross terms in Eq. B1, such as  $\log t_f \cdot \log Z$ , reduces the rms of the fit only marginally, by less than 0.01 mag, and that, therefore, the luminosity evolution  $E = m_V(t_f - t_{0.64}, Z) - m_V(t_f, Z)$  depends mainly on  $t_f$ , that is  $E \simeq E(t_f)$ .

The derivative of  $E(t_f)$  can be computed analytically from Eq. B1 and is given by the following equation:

$$F(t_f) = \frac{dE}{d \log t_f} = c_1 \cdot \left[ \frac{t_f}{t_f - t_{0.64}} - 1 \right] + 2c_2 \cdot \left[ \frac{t_f \cdot \log(t_f - t_{0.64})}{t_f - t_{0.64}} - \log t_f \right]. \quad (\text{B2})$$

This relation was used to compute the range of values of  $F(t_f)$  in section 3.2.

## REFERENCES

- Akritas, M.G., and Bershadsky, M.A. 1996, ApJ, 470, 706
- Barger, A.J., Aragón-Salamanca, A., Smail, I., Ellis, R.S., Couch, W.J., Dressler, A., Oemler, A., Poggianti, B.M., and Sharples, R.M. 1998, ApJ, 501, 522

- Bruzual, G.A., and Charlot, S. 1993, ApJ, 405, 538
- Busarello, G., Merluzzi, P., La Barbera, F., Massarotti, M., and Capaccioli, M. 2002, A&A, 389, 787
- Buzzoni, A. 1989, ApJS, 71, 817
- Capaccioli, M., Caon, N., and D’Onofrio, M. 1992, MNRAS, 259, 323
- Capelato, H.V., de Carvalho, R.R., and Carlberg, R.G. 1995, ApJ, 451, 525
- Dantas, C.C., Capelato, H.V., Ribeiro, A.L.B., and de Carvalho, R.R. 2002, MNRAS, in press (astro-ph/0211251)
- Fasano, G., Cristiani, S., Arnouts, S., and Filippi, M. 1998, AJ, 115, 1400
- Fasano, G., and Franceschini, A. 1987, MNRAS, 225, 155
- Graham, A. 2002, MNRAS, in press (astro-ph/0203509)
- Hamabe, M., and Kormendy, J. 1987, In: *Structure and Dynamics of Elliptical Galaxies*, IAU Symp., No.127, p.379, ed. de Zeeuw, T., Reidel, Dordrecht.
- Hoessel, J.G., Oegerle, W.R., and Schneider, D.P. 1987, AJ, 94, 1111
- Jørgensen, I., Franx, M., and Kjærgaard, P. 1995a, MNRAS, 273, 1097
- Jørgensen, I., Franx, M., and Kjærgaard, P. 1995b, MNRAS, 276, 1341
- Jørgensen, I., Franx, M., and Kjærgaard, P. 1996, MNRAS, 280, 167
- Jørgensen, I., Franx, M., Hjorth, J., and van Dokkum, P. G. 1999, MNRAS, 308, 833
- Kauffmann, G. 1996, MNRAS, 281, 487
- Kelson, D.D., Illingworth, G.D., van Dokkum, P.G., and Franx, M. 2000, ApJ, 531, 184
- Kjærgaard, P., Jørgensen, I., and Moles, M. 1993, ApJ, 418, 617
- Kormendy, J. 1977, ApJ, 218, 333
- La Barbera, F., Busarello, G., and Capaccioli, M. 2000, A&A, 362, 851
- La Barbera, F., Busarello, G., Merluzzi, P., Massarotti, M., and Capaccioli, M. 2002a, ApJ, 571, 790

- La Barbera, F., Merluzzi, P., Iovino, A., Busarello, G., Massarotti, M., and Capaccioli, M. 2002b, *A&A*, in press (astro-ph0211218)
- La Barbera, F., Busarello, G., Massarotti, M., Merluzzi, P., and Mercurio, A. 2002c, *A&A*, submitted (astro-ph0211478)
- Larson, R.B. 1974, *MNRAS*, 166, 585
- Lubin, L.M., and Sandage, A. 2001, *ApJ*, 121, 2289
- Lubin, L.M., and Sandage, A. 2001, *ApJ*, 122, 1071
- Lubin, L.M., and Sandage, A. 2001, *ApJ*, 122, 1084
- Lucey, J.R., Bower, R.G., and Ellis, R.S. 1991, *MNRAS*, 249, 755
- Massarotti, M., Iovino, A., Buzzoni, A., and Valls-Gabaud, D. 2001, *A&A*, 380, 425
- Mercurio, A., Girardi, M., Boschin, W., Merluzzi, P., and Busarello, G. 2002, *A&A*, in press (astro-ph0209536)
- Mobasher, B., Guzman, R., Aragon-Salamanca, A., and Zepf, S. 1999, *MNRAS*, 304, 225
- Pahre, M.A., Djorgovski, S.G., and de Carvalho, R.R. 1996, 456, 79
- Saglia, R. P., Bender, R., and Dressler, A. 1993, *A&A*, 279, 75
- Saglia, R.P., Bertschinger, E., Baggley, G., Burstein, D., Colless, M., Roger, L.D., McMahan, R.K., Jr., and Wegner, G. 1997, *ApJS*, 109, 79
- Sandage, A., and Lubin, L.M. 2001, *ApJ*, 121, 2271
- Sandage, A., and Perelmuter, J.-M. 1991, *ApJ*, 370, 455
- Schlegel, D.J., Finkbeiner, D.P., and Davis, M. 1998, *ApJ*, 500, 525
- Scodreggio, M., Giovanelli, R., and Haynes, M. P. 1997, *AJ*, 113, 101
- Scodreggio, M., Gavazzi, G., Belsole, E., Pierini, D., and Boselli, A. 1998, *MNRAS*, 301, 1001
- van Dokkum, P.G., Franx, M., Kelson, D.D., Illingworth, G.D., Fisher, D., and Fabricant, D. 1998, *ApJ*, 500, 714
- Ziegler, B.L., Saglia, R.P., Bender, R., Belloni, P., Greggio, L., and Seitz, S. 1999, *A&A*, 346, 13



Table 1. Samples used in the present study. Column 1: cluster identification. Column 2: redshifts. Column 3: waveband. Column 4: sample size. Columns 5, 6: limits in  $\langle \mu \rangle_e$  and magnitude. Column 7: references for data reduction and derivation of structural parameters with the following abbreviations: Jørgensen, Franx, and Kjærgaard (1995a,b); La Barbera et al. (2002a,b,c); Busarello et al. (2002), Mercurio et al. (2002, in preparation) (JFK95a,b; LBM02a; LMI02; LBM02c; BML02; MMM02).

	$z$	Waveband	N	$\langle \mu \rangle_{e,c}$	$m_c$	Ref.
COMA	0.023	$r_g$	72	...	15.3	JFK95a, JFK95b
A 209	0.21	R	81	20.1	20.1	MMM02, LBM02c
AC 118	0.31	R	101	20.8	20.8	BML02, LBM02a
EIS 0048	0.64	I	46	18.9	22.0	LMI02, LBM02c

Table 2. Slopes of the KR for COMA (JFK96), A 209, AC 118, and EIS 0048. Columns 2, 3 and 4 we list the values obtained by the different fitting procedures (see text), with the relative uncertainties ( $1\sigma$  standard intervals).

	$MLS_{\log r_e}$	$MLS_{\langle \mu \rangle_e}$	BMLS
COMA (JFK96)	$3.85 \pm 0.5$	$2.25 \pm 0.35$	$2.9 \pm 0.3$
A 209	$3.04 \pm 0.25$	$2.70 \pm 0.17$	$2.86 \pm 0.17$
AC 118	$2.84 \pm 0.20$	$2.67 \pm 0.15$	$2.74 \pm 0.16$
EIS 0048	$3.11 \pm 0.13$	$2.97 \pm 0.13$	$3.04 \pm 0.13$

Table 3. Mean values of the slope  $\beta$  of the KR obtained by the different fitting procedures. The uncertainties  $\sigma_\beta$  denote  $1\sigma$  standard intervals.

	$\beta$	$\sigma_\beta$
MLS <sub>log r<sub>e</sub></sub>	3.06	0.10
MLS <sub><math>\langle\mu\rangle_e</math></sub>	2.78	0.08
BMLS	2.91	0.08

Table 4. Zeropoint and scatter of the KR. Uncertainties denote  $1\sigma$  standard intervals.  $\sigma_{\langle\mu\rangle_e}$  is the observed scatter in  $\langle\mu\rangle_e$ , while  $\sigma_{\langle\mu\rangle_e}^{(i)}$  is the estimate of the intrinsic dispersion of the KR.

	$\alpha$	$\sigma_{\langle\mu\rangle_e}$	$\sigma_{\langle\mu\rangle_e}^{(i)}$
COMA (JFK96)	$18.79 \pm 0.08$	$0.45 \pm 0.05$	$0.34 \pm 0.07$
A 209	$18.95 \pm 0.08$	$0.51 \pm 0.04$	$0.32 \pm 0.06$
AC 118	$19.45 \pm 0.11$	$0.60 \pm 0.05$	$0.24 \pm 0.12$
EIS 0048	$19.51 \pm 0.07$	$0.42 \pm 0.04$	$0.29 \pm 0.06$

Table 5. Correction to restframe V-band for the cluster samples. Uncertainties denote  $1\sigma$  standard intervals.

	COR.
COMA (JFK96)	$-0.373 \pm 0.040$
A 209	$-0.527 \pm 0.004$
AC 118	$-0.450 \pm 0.020$
EIS 0048	$-1.095 \pm 0.030$

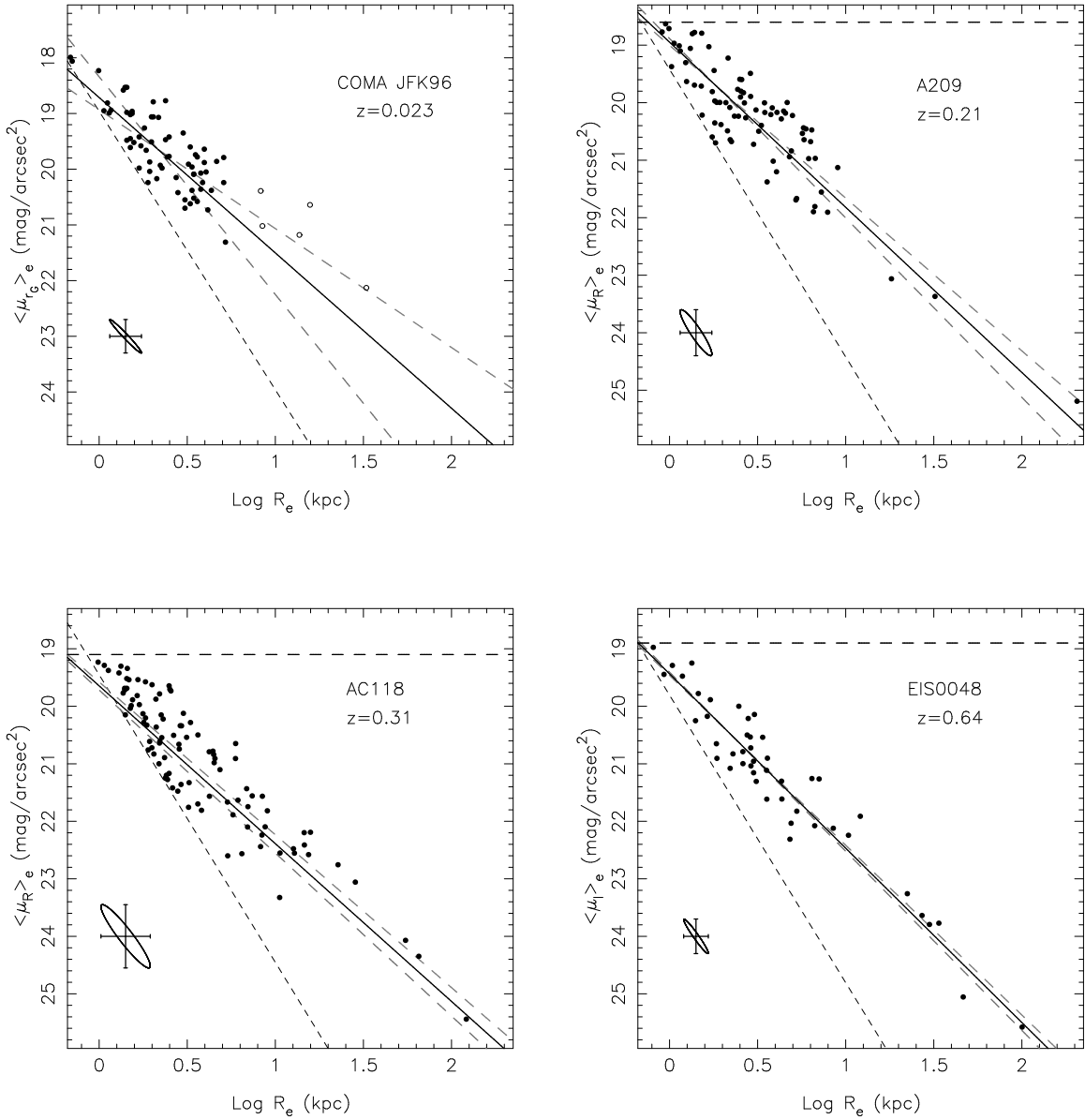


Fig. 1.— Kormendy relations for Coma, A209, AC118, and EIS0048. The range of  $\text{log } R_e$  is the same for each panel, while the range of  $\langle \mu \rangle_e$  is the same for A209, AC118, and EIS0048, and is shifted by  $-1 \text{ mag arcsec}^{-2}$  for Coma. The  $\text{MLS}_{\text{log } r_e}$  and  $\text{MLS}_{\langle \mu \rangle_e}$  fits are represented by the long-dashed lines, while the solid line is the BMLS regression. The short-dashed line and the horizontal line indicate the cuts in magnitude and  $\langle \mu \rangle_e$  for each sample. The correlation of the uncertainties on  $\text{log } r_e$  and  $\langle \mu \rangle_e$  are shown by the ellipses ( $1 \sigma$  confidence contours) in the lower-right of each panel. The galaxies that were not considered in the fits for the Coma cluster are marked by empty circles.

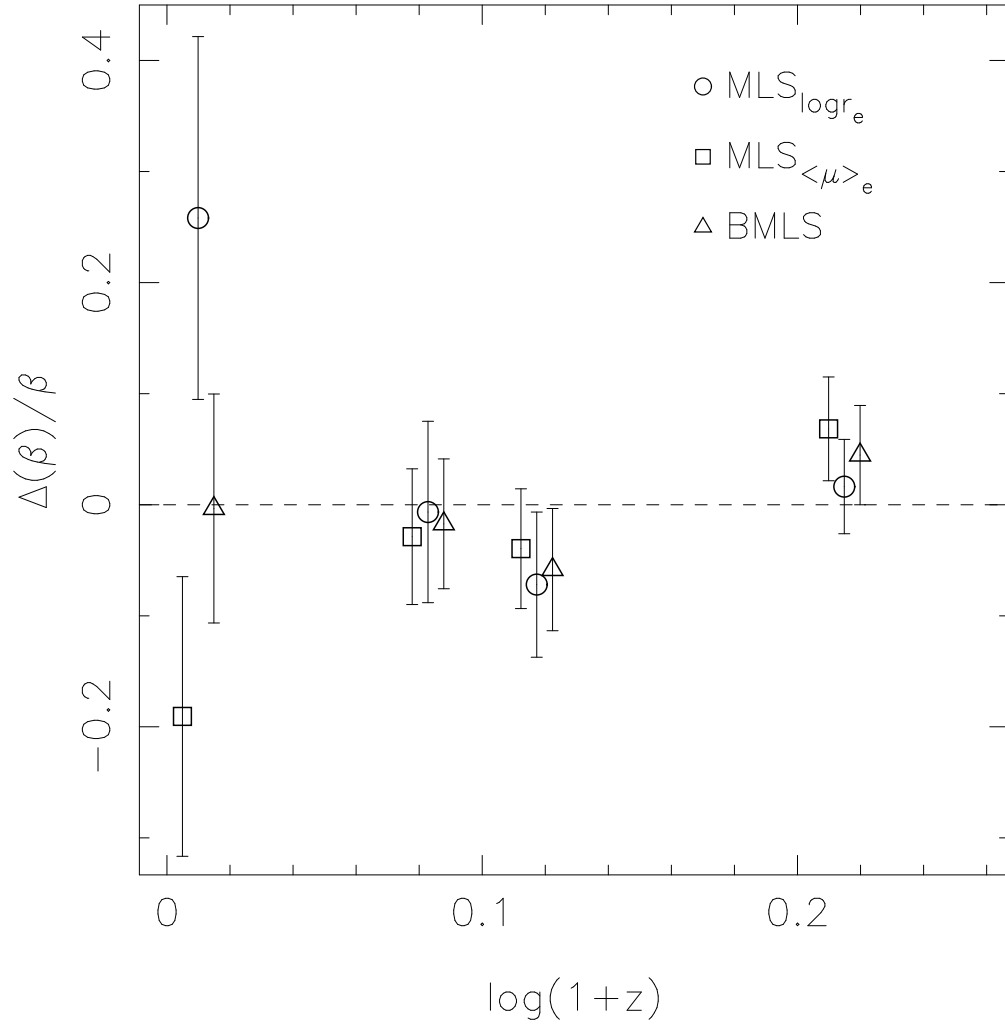


Fig. 2.— Evolution with redshift of the relative slope of the KR. The symbols denote the different fitting methods (see text).

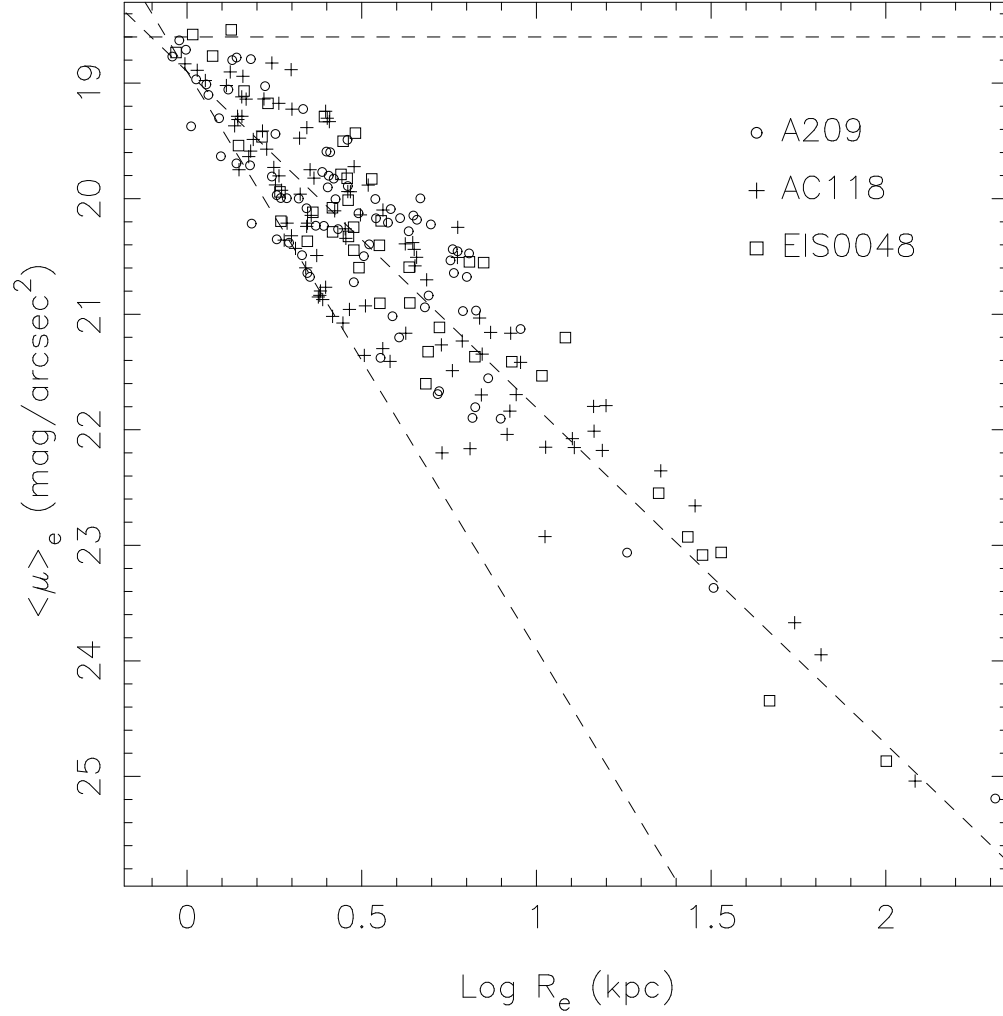


Fig. 3.— Kormendy relations of A 209, AC 118, and EIS 0048, shifted to the same zero point.

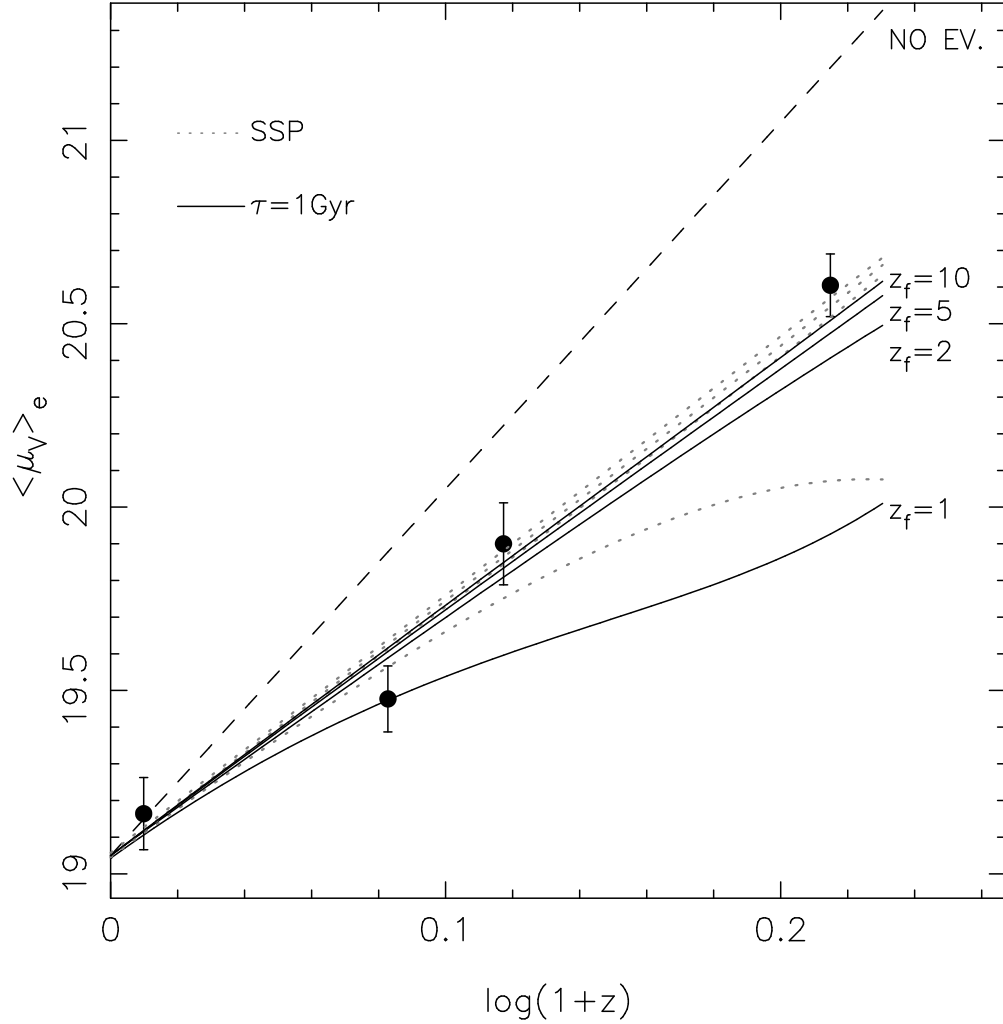


Fig. 4.— Evolution of the zeropoint of the KR as a function of redshift. The dashed line indicates the change for pure cosmological dimming. The other curves are dimming + passive evolution models corresponding to a SSP with formation redshifts  $z_f = 1, 2, 5, 10$  (dotted lines) and to a population with an exponential SFR ( $\tau = 1$  Gyr) starting at the redshifts used for the SSP (solid lines).

This figure "REMIE\_TOT.jpg" is available in "jpg" format from:

<http://arxiv.org/ps/astro-ph/0212294v2>